RSC Advances

This is an *Accepted Manuscript*, which has been through the Royal Society of Chemistry peer review process and has been accepted for publication.

Accepted Manuscripts are published online shortly after acceptance, before technical editing, formatting and proof reading. Using this free service, authors can make their results available to the community, in citable form, before we publish the edited article. This *Accepted Manuscript* will be replaced by the edited, formatted and paginated article as soon as this is available.

You can find more information about *Accepted Manuscripts* in the **Information for Authors**.

Please note that technical editing may introduce minor changes to the text and/or graphics, which may alter content. The journal's standard **Terms & Conditions** and the **Ethical guidelines** still apply. In no event shall the Royal Society of Chemistry be held responsible for any errors or omissions in this *Accepted Manuscript* or any consequences arising from the use of any information it contains.

Journal Name

ARTICLE

Feasible Nonaqueous Route to Synthesize High-Voltage Spinel Cathode Material for Lithium Ion Battery

Yi-Chun Jin and Jenq-Gong Duh[*]

High voltage spinels are of great interest as positive electrode materials for lithium-ion batteries in recent years. In this study, a new organic solvent system is explored for preparing this composite material via a co-precipitation process. The use of functional polymer surfactant significantly affects both structure and stoichiometry of spinel compounds in the non-aqueous batch. It was revealed that the residual halides and impurities can be completely eliminated at the precursor stage. A good cycling stability was demonstrated at room temperature and a greatly improved rate capability was successfully derived by this novel system as compared with the traditional aqueous system. The superior rate performance is mainly attributed to the appreciable formation of trivalences Mn, correlating to the change of Ni/Mn ordering and crystallographic phase transformation in the detailed structural analysis.

Introduction

Facing the current challenge of worldwide energy shortage and ever-increasing environment pollution, lithium ion battery is expected to play the crucial role as large-scale electrical storage device implemented in electric vehicles and modern electrical grid.[1, 2] In this content, the increasing demand of electrode material with high power density has attracted much investigations recently[3]. Among various cathode candidates, nickel substituted spinel ($LiNi_{0.5}Mn_{1.5}O_4$) has received extensive attentions due to its high re-dox plateau around 4.7 V during Li-intercalations [4, 5]. The ultimate working potential elevates the overall energy output and increases the possibility of high power delivery.

A variety of methods have been examined to prepare the cathode compound, such as solid-state reaction[6], sol–gel[7], emulsion drying[8], hydrothermal[9], molten salt[10], combustion[11] and spray pyrolysis[12]. Comparing with a wide variety methods, co-precipitation process is known as a preferable process for synthesizing multicomponent materials.[13, 14] In most cases, the precursor route of co-precipitation process is under an aqueous system.[15, 16] The low boiling point of water limits the reaction kinetic of metathesis below 100 ºC. In addition, the hydrophilic interaction between metal salt and precipitator usually causes localized aggregation after water vaporizations, leading to nonstoichiometric products[17]. Moreover, some inorganic precipitant are used in aqueous system to obtain the hydroxide precipitation, followed by repeated filtering to get rid of residual alkaline or halogen ions[18]. Apart from aqueous chemistry, few methodologies have been reported for non-aqueous synthesis of multicomponent metal oxides, still less studies with deeper discussion on polymeric surfactants are used or not.

In a solvent-controlled synthetic approach, the organic solvent acts as both reactant and control agent for particle growth.[19,20] The reactivity of metal oxide precursors in organic solvent is greatly decreased under the exclusion of water[21], therefore, makes it easier to control the particle sizes. The role of organic species in co-precipitation approaches is rather complex, however, it can be organized into several steps[22]: (1) metathesis reaction of metal salts and reagents, (2) condensation of carboxylate groups, (3) formation of nanometric framework and (4) elimination of alkyl halide.

DMAc (dimethylacetamide) is a dipolar, aprotic solvent with great solving power for high molecular-weight polymers and good miscibility with a wide range of organic and inorganic compounds.[23] The polar nature of DMAc enables it to act as a combined solvent in catalyst reactions.[24] Furthermore, its boiling point (166ºC) allows reactions to be carried out at much higher temperatures without the need to operate under pressure. Polyamic acid is an intermediate product for manufacture of polyimide.[25] It preserves strong hydrogen bonds and good solubility in organic solvent.

In this study, DMAc solvent is first employed in co-precipitation process to fabricate spinel compounds. The pre-mediate of polyamic acid was found necessary for synthesizing pure-phase spinel compound in the non-aqueous system. As applied precipitator, oxalic acid is a strong ligand for transition metal ion. It allows to acidizes ionic halides into volatile hydroxyl gases easily.[26] Since both the surfactant and the precipitator can be easily removed through heating process, the repetitive filtration step can be eliminated. All experimental results were compared to the sample fabricated in an aqueous system, regarding morphology, crystal structure, composition and electrochemical performances.

Department of Materials Science and Engineering, National Tsing Hua University, Hsinchu, 30013, Taiwan. E-mail: jgd@mx.nthu.edu.tw; s9931512@m99.nthu.edu.tw; Tel: +886-3-5712686.

Experimental

Synthetic procedures

Dehydrate metal chlorides (LiCl, MnCl$_2$, and NiCl$_2$) were used as cationic sources with a stoichiometric ratio (Li: Ni: Mn= 2: 1: 3). Initially, the dark blue solution was obtained as precursor powder dissolved in a DMAc solvent. After ultrasonic vibration, the solution colour completely transferred to a transparent green. Afterward, appropriate amount of polyamic acid (M.W=10,000~50,000) was added into the previous solution with continuously stirring for 1h to assure the homogeneous reaction. Then, oxalic acid was slowly dripped into the former solution route while the temperature was kept around 150°C. The solution eventually turned into a jelly-like substance with pale green colour. The viscous mixture was vacuum dried at 250 °C for 3h to yield the polymeric matrix. Finally, the dried compound underwent two-step calcinations in ambient atmosphere (first step: 400 $^{\circ}$C for 3 h, second step: 700 $^{\circ}$C for 10 h). A prolong annealing time is sufficient for crystallization of spinel framework[27]. As-fabricated samples with/without the pre-mediation of polymer are denoted as NAQ-P/NAQ, respectively. All the aforementioned process was identically repeated in the aqueous system as for comparison, whereas the resulting sample is denoted as "AQ". Unlike DMAc system, the temperature of aqueous mixing has to be limited below 100 $^{\circ}$C for preventing water dissipations.

Materials characterization

Powder X-ray diffraction (Rigaku-6000, Cu-Kα radiation) was recorded by an automated diffractometer with step size and exposure time set as 0.02 ° and 4 s, separately. The sample morphology was observed by In-lens thermal field emission scanning electron microscope (JSM-7600, JOEL) with high probe current energy dispersive X-ray spectrometer. Thermogravimetric analyzer (TGA-7, Perkin Elmer) was performed under air flow of 20 mL·min^{-1} with a heating rate of 10 °C·min^{-1}. Fourier transform infrared spectroscopy analysis (Perkin-Elmer, Horiba F730) was carried out in a wavelength range from 400 to 700 cm^{-1} with a spectral resolution of 4 cm^{-1}. The sample pellet was prepared by diluting the prepared powder with ten times KBr in volume. X-ray photoelectron analysis was carried out by Ulvac-PHI (PHI 1600) electron spectrometer at a base pressure in the analysis chamber of 5x10^{-10} pa (during the measurement 1.5x10^{-9} pa) with Mg Kα X-ray source (excitation energy hν = 1253.6 eV). The energy scale and shifts is corrected to the C1s peak maximum at 285 eV for electrostatic charging. The instrumental resolution measured as the full width at a half-maximum (FWHM) is 1.88 eV. The integrated fitting of the recorded XPS spectra was performed, using a symmetrical Gaussian-Lorentzian curve after a Shirley-type subtraction of the background by Xpspeak41 software.

Electrochemical measurement

80 wt.% as-prepared materials were mixed with 13 wt.% carbon black and 7 wt.% polyvinylidenefluoride (PVDF) in N-methylpyrrolidinone (NMP) for fabrication of cathode electrodes,. The slurry underwent 2 hour ball-milling, and was then casted onto an Al-foil afterward. The loading of as-fabricated cathode electrodes was in a range of 2.2 to 2.5 mg·cm^{-2} for both AQ and NAQ-P. The 2032 type coin cell was assembled in an argon-filled glove box with a controlled atmosphere, whereas both H$_2$O and O$_2$ were under 0.1 ppm. For the half-cell test, lithium metal as negative electrodes and Celgard 2400 membrane as separators in an electrolyte mixture. The 1 M LiPF$_6$ was dissolved in 1: 2 volume ratio of ethylene carbonate (EC)/dimethyl carbonate (DMC). Arbin battery testing system (BT-2000) was employed with a constant current density ranging from 0.9 to 0.7 mA·cm^{-2} with the cut-off voltage between 3.5 to 5 V. The electrochemical behaviour of sample was evaluated by cyclic voltammetry (Potentiostat 263A) at a voltage sweep rate of 0.1 mVs^{-1}.

Results and discussion

Fig. 1 shows SEM image of as-calcined powder samples AQ, NAQ and NAQ-P prepared by the different solvent systems (ie. aqueous, non- aqueous and non-aqueous with polymer assisted). A well-shaped octahedral particle was observed in both samples of NAQ-P and AQ with the comparable size around 300 nm. Nevertheless, the chunky-like powder was found in sample NAQ with an average particle size about 4 μm. The measured particle size is widely ranged from 0.5 to 10 μm with a serious powder aggregation
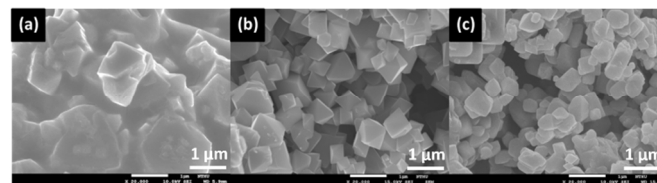
Fig. 1 SEM images of as-fabricated sample: (a) NAQ, (b) AQ, and (c) NAQ-P.

The composition of as-fabricated samples was confirmed by XPS analysis and the calculated Mn/Ni stoichiometry is displayed in Table 1. The calculation is based on the equation: $(n_1/n_2)=(I_1/S_1)/(I_2/S_2)$, where n is atomic concentration, I is integrated peak area and S is relative sensitivity factor (R.S.F.) of elements (S=2.66 for Mn 2p$_{3/2}$ and 4.04 for Ni 2p$_{3/2}$)[28]. The correspondence pattern with the fitting curve is provided in supporting information. The result shows that the atomic ratio of Mn/Ni in three samples are close to 3, coincidences to our original design of LiNi$_{0.5}$Mn$_{1.5}$O$_4$. It was also noticed an obvious chloride contamination in sample NAQ. Yet, none of any chloride contents can be detected in both samples AQ and NAQ-P as evidenced in Fig.2.

Table 1. XPS analysis of as-fabricated sample powders

Sample	Integrated peak area in elemental XPS spectrum			Atomic ratio of Mn/Ni	Relative atomic % of Cl
	Mn 2p$_{3/2}$	Ni 2p$_{3/2}$	Cl 2p$_{3/2}$		
AQ	8510.6	4312.7	0	2.98	n/a
NAQ	7286.3	3913.5	353.7	2.82	7.48
NAQ-P	8903.1	4425.4	0	3.02	n/a
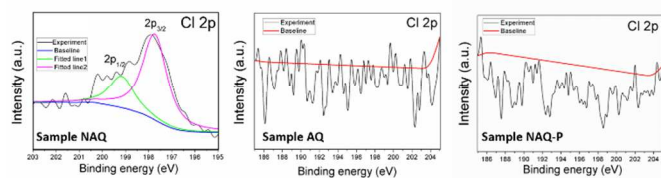
Fig. 2 XPS spectra of Cl 2p in as fabricated powder samples

The following mechanism may help to explain the variation on Cl contents. During co-precipitations, the spontaneous metathesis occurred between oxalic acid and metal salt, releasing hydrochloric acid according to the reaction: $2LiCl + NiCl_2 + MnCl_2 + 3H_2C_2O_4 \rightarrow Li_2C_2O_4 + NiC_2O_4 + MnC_2O_4 + 6HCl$. In DMAc solvent system, however, the undesired side reaction was produced as follows: $CH_3CON(CH_3)_2 + H_2O + HCl \rightarrow CH_3COOH + (CH_3)_2NH_2^+Cl^-$. The N, N-disubstituted amide would hydrolyze in the presence of hydrochloric acid, leaving the intermediate compound "$(CH_3)_2NH_2Cl$" [29]. This compound is hard to remove through high temperature calcination process. Furthermore, the fore reaction easily take places if any water retains.

It is noteworthy that after mediating polyamic acid, none of any residual chlorides can be detected in the sample NAQ-P. The transformation is attributed to the intermolecular capping between metal-DMAc complex and polyamic acid in the precursor stage. A study suggested that DMAc behaves as a neutral ligand and forms a complex between metal ions proposed by reaction: $MeCl_x + 2x\ DMAc_{(excess)} \rightarrow [Me(DMAc)_{2x}]Cl_x + DMAc_{(excess)}$. [30]

Due to the anionic valences of polymeric chain, carboxylic moieties of polyamic acid reacts with metal-DMAc to satisfy its cationic valencies. This process accompanied with liberating of gaseous HCl.[31] The whole chelating process is illustrated in Fig. 3.
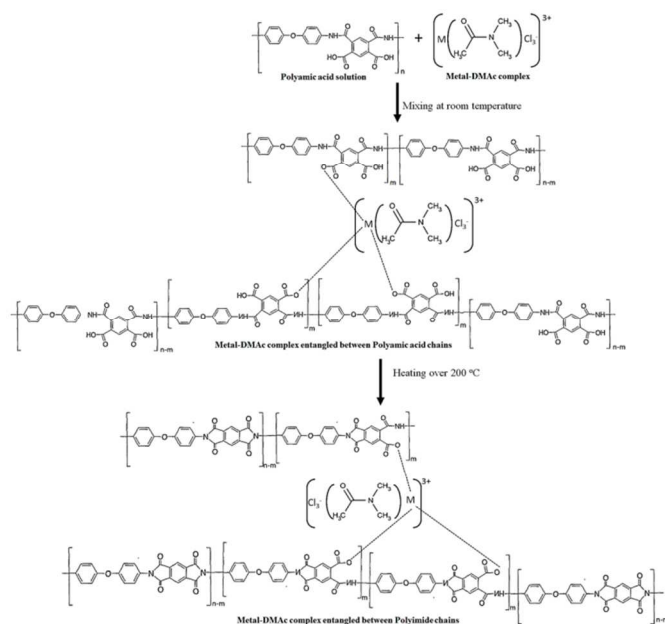
Fig.3 Schematic illustration of polyamic acid capping with metal-DMAc complex in a co-precipitation route.

Therefore, none of any residual chlorides was trapped in the resulting product (sample NAQ-P) after polymer pre-meditations. In addition to the remove of contamination, significant reduction of particle size was also obtained via introducing polymeric surfactants. Previous results strongly support the founding that polymers can form a barrier which hinders the particle growth and inhibits particle aggregations. [32, 33] The process is based on the chemical adsorption between metal oxalates and polymer surface, creating a shield to against van der Waals interactions between particles. [34, 35]

Fig. 4 displays the X-ray diffraction pattern of powder samples fabricated by different solvent systems. Both samples of NAQ-P and AQ were indexed as a perfect cubic spinel structure (JCPDS:32-0581) without any undesired secondary phases. Referring to the spectra derived from XPS, this result implies that the stoichiometric component— $LiNi_{0.5}Mn_{1.5}O_4$ is successfully achieved. Nevertheless, the noticeable secondary phases were found in sample NAQ, together with unexpected phase separations such as Mn_2O_3 and $LiNiO_x$. It is assumed that the pre-mediating of chloride impurity obscures the interatomic diffusion of metal ions during sintering process, leading to the destruction of spinel framework.
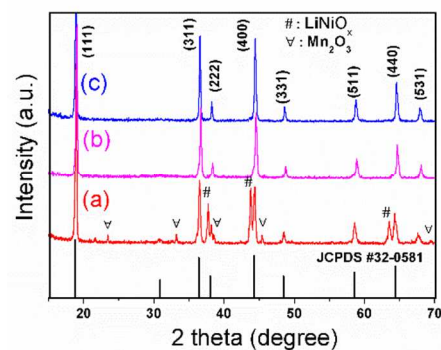
Fig. 4 X-ray diffraction patterns of powder sample: (a) NAQ, (b) AQ, and (c) NAQ-P.

The dependence between ordered/disordered distributions of Ni/Mn atoms on the octahedral sites has been reported with a significant effect on its electrochemical properties.[36, 37] Spinel $LiNi_{0.5}Mn_{1.5}O_4$ has two different crystallographic phases ($P4_332$ and Fd-3m) each corresponds to the specific X-ray diffraction patterns (JCPDS #80-2184 and #32-0581). The calculated peak ratio of I_{111}/I_{311} is a useful indicator to distinguish these two structures in spinel samples. The (311) diffraction peak reflects the displacement of A/B atoms in AB_2O_4 formula of antispinel structure[38], which suggests the tendency to form Fd-3m phase. As listed in Table 2, I_{111}/I_{311} ratio of sample AQ and NAQ-P is 2.27 and 1.72, respectively. This indicates that the crystallographic phase of samples AQ and NAQ-P separately belongs to $P4_332$ and Fd-3m. Moreover, the intensity ratio of I_{311}/I_{400} reflects the degree of tetragonal distortion from cubic spinel structure.[39] The phase transition of spinel $LiNi_{0.5}Mn_{1.5}O_4$ from $P4_332$ to Fd-3m is triggered by the creation of multi-valences Mn. [40, 41] The expansion of lattice parameter in sample NAQ-P is therefore associated with the numerous presence of Mn^{3+}, due to bigger ionic radius of Mn^{3+} (0.65 Å) than Mn^{4+}(0.54 Å).

Table 2. Comparison of peak intensity ratio and lattice parameters of X-ray diffraction patterns

Sample	Lattice param-eter (Å)	Relative intensity (Normalized by I_{111})			Intensity ratio	
		I_{111}	I_{311}	I_{400}	I_{111}/I_{311}	I_{311}/I_{400}
AQ	8.139	100	43.9	48.0	2.27	0.91
NAQ-P	8.199	100	57.9	56.7	1.72	1.02
JCPDS #32-0581	8.173	100	55.0	60.0	1.67	0.92
JCPDS #80-2184	8.170	100	38.2	42.6	2.61	0.89

To further understand the crystallographic properties of spinel samples, FTIR spectroscopy was employed in this study. It is proved to be an effective technique to differentiate ordered and disordered structures in $LiNi_{0.5}Mn_{1.5}O_4$.[42, 43] Spinel $LiNi_{0.5}Mn_{1.5}O_4$ with ordered cation occupancy exhibits a series of fingerprint bands at 432, 476, 501, 557, 588, 623, and 647 cm^{-1} as displayed in Fig. 5. Apparent shoulder bands at 647 and 432 cm^{-1} represents a higher degree of Ni/Mn ordering, associating to the $P4_332$ phase.[44] Moreover, an increased ratio of I_{588}/I_{623} is also distinguished as a higher ordered Ni/Mn occupancy in spinel lattice.[45] It clearly reveals a higher cation order of $P4_332$ phase in sample AQ with respect to $Fd-3m$ phase in sample NAQ-P, in consist of the result of X-ray analysis. The obvious phase transformation is correlated with the increasing amount of Mn^{3+} in spinel structure[46], as evidenced in the following cyclic voltammetry analysis.
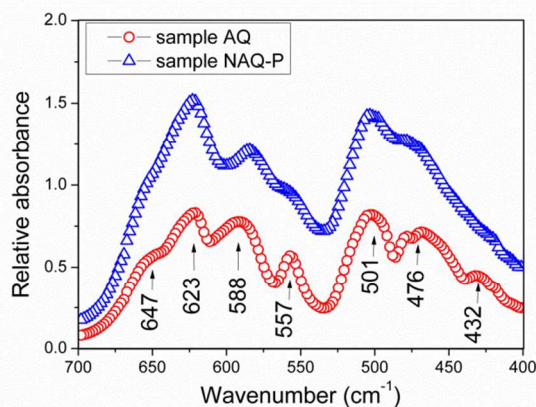
Fig. 5 FTIR spectra of samples AQ and NAQ-P.

Fig. 6 (a) displays room temperature electrochemical performances of assembled NAQ-P and AQ half-cells. Both samples demonstrated a competitive capacity retention during charge-discharge in 1C. A similar initial capacity around 128-125 $mAhg^{-1}$ was delivered and losses about 15 % after 250 cycles. With increasing discharge rate (1, 10, 20 C), the superior high current stability was delivered in sample NAQ-P rather than sample AQ as shown in Fig. 6 (b). Sample NAQ-P outperforms about 85 % initial capacity during 10 C discharging. Even at 20 C, it still remained a half of the specific discharge capacity around 60 $mAhg^{-1}$. Table 3 lists the performance of $LiNi_{0.5}Mn_{1.5}O_4$ cathodes in comparison with related literatures at room temperature. Among various co-precipitation routes, the optimal rate capability is revealed in this study while discharging the spinel electrode at 5C and 10C.

Table 3. Comparison of room temperature performances in high voltage spinels synthesized by various co-precipitation route

Various co-precipitation route	Year published	Initial capacity in 1C ($mAhg^{-1}$)	C-rate capability (Discharge rate: $mAhg^{-1}$)
This work	*2014*	*125-120*	*5C: 110-100* *10C: 65-60*
Ethanol[33]	2013	130-125	5C: 90-100 10C: 55-60
Distilled water[13]	2010	132-130	5C: 45-40 10C: 25-20
Distilled water[14]	2009	130-128	3C: 125-110 5C: 100-90
Distilled water with ultrasonic-assisted[16]	2007	120-115	1C: 120-115 2C: 110-100
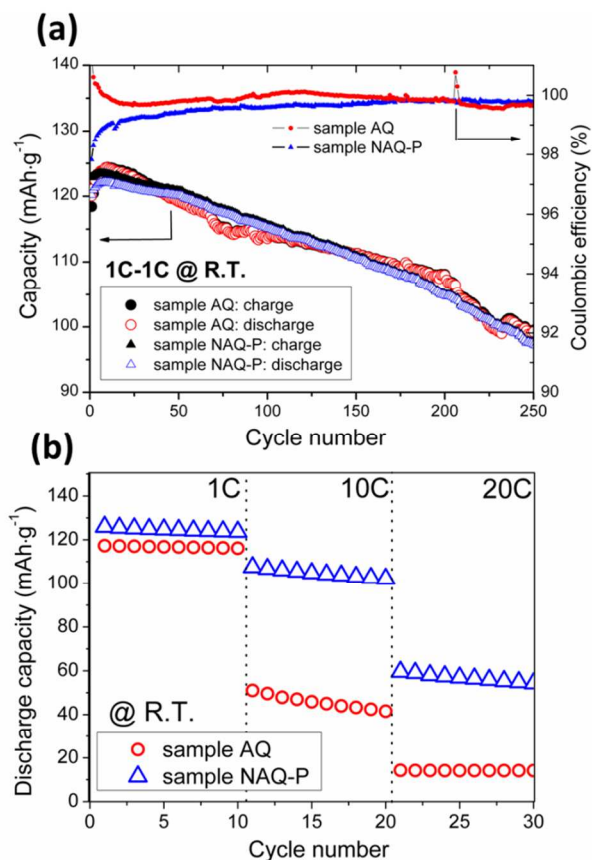
Fig. 6 Electrochemical properties of samples AQ and NAQ-P in half-cells (a) cycling performance and (b) rate performances at room temperature.

The cyclic voltammetry was applied for examining detail electrochemistry of assembled cells. The specialized reduction-oxidation peak of $LiNi_{0.5}Mn_{1.5}O_4$ was around 4.7 V, corresponding to Ni^{2+}/Ni^{4+} symmetric reaction. Additionally, an obvious re-dox peak at 4 V was recorded at sample NAQ-P as

exhibited in Fig. 7. The small bump corresponds to Mn^{3+}/Mn^{4+} symmetric reaction.[47] Conclusively, the remarkable rate capability of sample NAQ-P is mainly attributed from two factors. An improved electric conductivity due to a higher Mn^{3+} contains and the site disorder of Ni/Mn in spinel structure[48]. These two factors facilitate phase transformations during lithium intercalation which is inseparable in the spinel $LiNi_{0.5}Mn_{1.5}O_4$ system. [49, 50]
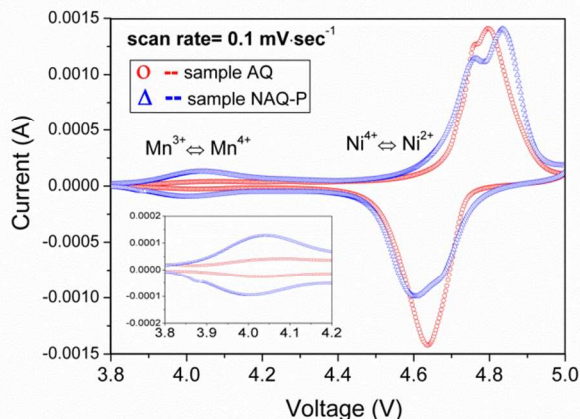
Fig. 7 Cyclic voltammetry of samples AQ and NAQ-P in scan rate of 0.1 mV·s⁻¹

Conclusions

The use of organic solvent in co-precipitation process is a newly adapted for synthesizing cathode compound materials. Through incorporation of specialized polymeric surfactant at the precursor stage, a well-crystallized fine powder with pure spinel phase was successfully obtained. Moreover, the residual halide impurities, such as chlorides, could be eliminated completely without additional filtrations. The adequate cycling stability is demonstrated and superior rate capability is derived as compared to the traditional aqueous system. Expand from this concept, a new class of co-precipitation method could be therefore developed. It clearly represents a feasible method for solvent control and an alternative use of polymeric surfactants. The accomplished compound product is potentially expected to be further used in functionalized lithium insertion material for future applications.

Acknowledgements

References

1   M. M. Thackeray, C. Wolverton and E. D. Isaacs, *Energy Environ. Sci.* , 2012, **5**, 7854-7863

2   Z. Yang, J. Zhang, C. W. Michael, X. Lu, D. Choi, J. P. Lemmon and J. J. Liu, *Chem. Rev.*, 2011, **111** (5), 3577-3613

3   J. B. Goodenough and Y. Kim, *Chem. Mater.*, 2010, **22**, 587−603.

4   R. Santhanam and B. Rambabu, *J. Power Sources,* 2010, **195**, 5442-5451

5   M. Kunduraci, J. F. Al-Sharab and G. G. Amatucci, *Chem. Mater.*, 2006, **18**, 3585-3592

6   Z. Chen, H. Zhu, S. Ji, V. Linkov, J. Zhang and W. Zhu, *J. Power Sources*, 2009, **189**, 507-510

7   Y. Lee, J. Mun, D. W. Kim, J. K. Lee and W. Choia, *Electrochim. Acta* 2014, **115**, 326-331

8   X. Zhang, F. Cheng, J. Yang and J. Chen, *Nano Lett.*, 2013, **13** (6), 2822-2825

9   X. Huang, Q. Zhang, J. Gan, H. Chang and Y. Yang, *J. Electrochem. Soc.*, 2011, **158** (2), A139-A145

10   J. H. Kim, S. T. Myung and Y. K. Sun, *Electrochim. Acta*, 2004, **49** (2), 219-227

11   L. Zhang, X. Lv, Y. Wen, F. Wang and H. Su, *J. Alloys and Compounds,* 2009, **480**, 802-805

12   S. H. Choi, Y. J. Hong and Y. C. Kang, *Nanoscale*, 2013, **5**, 7867-7871

13   D. Liu, J. Han, J. B. Goodenough, *J. Power Sources,* 2010, **195**, 2918-2923

14   X. Fang, N. Ding, X. Y. Feng, Y. Lu and C.H. Chen, *Electrochimi. Acta*, 2009, **54**, 7471-7475

15   Y. H. Ding, H. M. Ren, Y. Y. Huang, F. H. Chang, X. He, J. Q. Fen and P. Zhang, *Nanotechnology*, 2013, **24**, 375-401

16   T. F. Yi, X. G. Hu, *J. Power Sources*, 2007, **167**, 185-191

17   Y. Fan, J. Wang, X. Ye and J. Zhang, *J. Mater. Chem. Phys.*, 2007, **103**, 19-23

18   Z. Li, N. A. Chernova, J. Feng, S. Upreti, F. Omenya and M. S. Whittingham, *J. Electrochem. Soc.*, 2012, **159**, A116−A120

19   M. Niederberger and G. Garnweitner, *Chem. Eur. J.*, 2006, **12**, 7282-7302

20   Y. W. Jun, J. S. Choi and J. Cheon, *Angew. Chem. Int.*, 2006, **45**, 3414-3439

21   M. Karmaoui, M. G. Willinger, L. Mafra, T. Herntricha and N. Pinna, *Nanoscale*, 2009, **1**, 360–365

22   X. R. Ye, D. Z. Jia, J. Q. Yu, X. Q. Xin and Z. Xue, *Adv. Mater.*, 1999, **11**, 941-942

23   A. Potthast, T. Rosenau, R. Buchner, T. Röder, G. Ebner, H. Bruglachner, H. Sixta, P. Kosma, *Cellulose*, 2002, **9**, 1, 41-53

24   G. Pistoia, B. Scrosati, *Ric. Sci.*, 1967, **37**, 1173-1175

25   H. Yamada, M. Fukudome, N. Egawa, Method for Producing Polyimide Film, 2001, *US6264866*

26   H. Fang, L. Li and G. Li, *J. Power Sources*, 2007, **167**, 223-227

27   N. M. Hagh and G. G. Amatucci, *J. Power Sources*, 2010, **195**, 5005-5012

28   B.V. Cris "Handbooks of Monochromatic XPS Spectra: The Elements and Native Oxides-Volume 1" *XPS International LLC: Mountain View*, 2004, CA, USA

29   S. Zen and E. Kaji, *Org. Synth.*, 1977, **57**, 60.

30   L. T. Taylor and R. K. Boggess, *J. Polym. Sci. Part. A.*, *Polym. Chem.* 1987, **25**, 685.

31   C. Kundnani, A. K. Gupta, M. Arya, D. Shrivastava, P. Aseri, J. Keller and R. Bajpai, *Polym. Eng. Sci.*, 2009, **49**, 977-983

32   Y. C. Jin and J. G. Duh, *Mater. Lett.*, 2013, **93**, 77-80

33   W. Liu, G. C. Farrington, F. Chaput and B. Dunn, *J. Electrochem. Soc.*, 1996, **143** (3), 879-884

34   J. Huang, N. Matsunaga, K. Shimanoe, N. Yamazoe and T. Kunitake, *Chem. Mater.*, 2005, **17**, 3513-3518

35   J. C. Arrebola, A. Caballero, M. Cruz, L. Hernán, J. Morales and E. R. Castellón, *Adv. Funct. Mater.,* 2006, **16**, 1904-1912

36   S. Ivanova, E. Zhecheva, R. Stoyanova, D. Nihtianova, S. Wegner, P. Tzvetkova and S. Simova, *J. Phys. Chem. C*, 2011, **115**, 25170-25182

37   J. Zheng, J. Xiao, X. Yu, L. Kovarik, M. Gu, F. Omenya, X. Chen, X. Q. Yang, J. Liu, G. L. Graff, M. S. Whittingham and J. G. Zhang, *Phys. Chem. Chem. Phys.*, 2012, **14**, 13515-13521

38   J. Feng, Z. Huang, C. Guo, N. A. Chernova, S. Upreti and M. S. Whittingham, *ACS Appl. Mater. Interfaces*, 2013, **5**, 10227−10232

39   Z. Bai, N. Fan, Z. Ju, C. Sun, Y. Qian, *Mater. Lett.* 2012, **76**, 124−126.

40   J. Xiao, X. Chen, P. V. Sushko, M. L. Sushko, L. Kovarik, J. Feng, Z. Deng, J. Zheng, G. L. Graff, Z. Nie, D. Choi, J. Liu, J. Zhang and M. S. Whittingham, *Adv. Mater.*, 2012, **24**, 2109−2116

41   H. Seyyedhosseinzadeh, F. Mahboubi and A. Azadmehr, *Electrochim. Acta*, 2013, **108**, 867- 875

42   K. Ariyoshi, Y. Iwakoshi, N. Nakayama and T. Ohzuku, *J. Electrochem. Soc.*, 2004, **151**, A296−A303.

43   J. H. Kim, C. S. Yoon, S. T. Myung, Jai Prakash and Y. K. Sun, *Electrochem. Solid-State Lett.*, 2004, **7** (7), A216-A220

44   T. F. Yi and Y. R. Zhu, *Electrochim. Acta*, 2008, **53**, 3120-3126

45   X. Ma, B. Kang and G. Ceder, *J. Electrochem. Soc.*, 2010, **157** (8), A925-A931

46   Y. C. Jin, C. Y. Lin and J. G. Duh, *Electrochim. Acta*, 2012, **69**, 45-50

47   D. Liu, W. Zhu, J. Trottier, C. Gagnon, F. Barray, A. Guerfi, A. Mauger, H. Groult, C. M. Julien, J. B. Goodenough and K. Zaghib, *RSC Adv.*, 2014, **4**, 154-167

48   M. Kunduraci and G. G. Amatucci, *J. Electrochem. Soc.*, 2006, **153** (7), A1345−A1352

49   J. Xiao, X. Chen, P. V. Sushko, M. L. Sushko, L. Kovarik, J. Feng, Z. Deng, J. Zheng, G. L. Graff, Z. Nie, D. Choi, J. Liu, J. G. Zhang and M. S. Whittingham, *Adv Mater.*, 2012, **24** (16), 2109-2116.

50   J. H. Kim, S. T. Myung, C. S. Yoon, S. G. Kang and Y. K. Sun, *Chem. Mater.*, 2004, **16**, 906-914